NACA TN 2605

TECH LIBRARY KAFB, NM
0065709

NATIONAL ADVISORY COMMITTEE FOR AERONAUTICS

TECHNICAL NOTE 2605

BEHAVIOR OF VORTEX SYSTEM BEHIND CRUCIFORM WINGS - MOTIONS OF FULLY ROLLED-UP VORTICES

By Alvin H. Sacks

Ames Aeronautical Laboratory
Moffett Field, Calif.

Washington
January 1952

AFMDC
TECHNICAL LIBRARY
AFL 2811

TECH LIBRARY KAFB, NM

0065709

.K

NATIONAL ADVISORY COMMITTEE FOR AERONAUTICS

TECHNICAL NOTE 2605

BEHAVIOR OF VORTEX SYSTEM BEHIND CRUCIFORM WINGS - MOTIONS OF FULLY ROLLED-UP VORTICES

By Alvin H. Sacks

SUMMARY

The motions of four fully rolled-up vortices representing the vortex system trailing behind cruciform wings are studied by theoretical and visual-flow methods. The analysis applies throughout the Mach number range.

Equations are developed for the three-dimensional paths traced by the vortices behind a cruciform wing banked 45°, and calculations are made of the distance behind the wing at which the upper two vortices pass through the lower two. It is found that this "leapfrog" distance depends upon the lift coefficient, aspect ratio, and span loading of the cruciform wing, and that for low-aspect-ratio cruciform wings leapfrogging may occur within two chord lengths of the trailing edges.

The various types of vortex motion to be expected throughout the angle-of-attack range are considered in some detail, and the interaction of the two vortex sheets shed from the cruciform wing is taken into account. Results of some water-tank studies are also presented and compared with the theory.

INTRODUCTION

The downwash behind plane wings has been studied theoretically by a number of authors and considerable attention has been given to the rolling up of the trailing vortex sheet. The analysis of Kaden (reference 1) predicted the distance behind the wing at which the sheet may be considered to be fully rolled up into two trailing vortices, and this work was later used (in reference 2) to demonstrate the usefulness of the single horseshoe-vortex approximation for the calculation of the downwash behind wings of low aspect ratio. Since at the present time cruciform configurations are largely confined to wings of low aspect ratio, the rolling up of the trailing vortex sheets is again of major concern, and the behavior of the fully rolled-up vortices is again of considerable interest.

While in the case of the plane wing the vortex sheet became rolled up into a vortex pair which simply moved downward at a uniform speed at great distances behind the wing, the analogous problem for cruciform wings is necessarily more complicated. Instead of the two rolled-up vortices, there are now presumably four (one from each wing panel) and their induced effects upon one another are such as to produce quite intricate paths of motion. The downwash field, of course, may therefore become extremely involved. This report is concerned with a study of the motions of the four rolled-up vortices and their effect on the downwash behind cruciform wings.

SYMBOLS

A aspect ratio $\left(\frac{b^2}{S}\right)$

b span of one wing $(2s_o)$

c root chord

C_L lift coefficient of cruciform wing $\left(\frac{L}{qS}\right)$

C_L' lift coefficient of plane wing $\left(\frac{L'}{qS}\right)$

c_l section lift coefficient for plane wing

d distance behind wing trailing edge

d_L distance behind wing trailing edge where four rolled-up vortices are collinear (leapfrog distance)

f constant of the motion related to distance between centers of gravity of two vortex systems $(y_1 + y_2)$

G parameter which depends on initial vortex positions

$$\left[\frac{1}{\frac{y_o}{f}\left(1 - \frac{y_o}{f}\right)} - 2\right]$$

L lift of cruciform wing

L' lift of plane wing

M free-stream Mach number

q free-stream dynamic pressure $\left(\frac{1}{2}\rho U^2\right)$

Q^2 parameter used for periodic motion $\frac{f^2(4-G)}{4G}$

$\bar{Q}^2$ parameter used for aperiodic motion $(-Q^2)$

R^2 $\dfrac{f^2G}{4(G + 4)}$

S area of one wing

s local semispan of one wing

s_o maximum semispan of one wing

s' semispan of rolled-up vortices from one wing

t time

U free-stream velocity

v velocity of vortex center in y direction

w velocity of vortex center in z direction

x,y,z right-hand orthogonal coordinates with x axis in stream direction

y_o, z_o initial values of y_1 and z_1

$z_{1,2}$ vertical distance between vortices 1 and 2 (See sketch on page 9.)

α angle of attack of cruciform wing axis

α' angle of attack of one wing

β angle of sideslip of one wing

γ ratio of vortex strengths $\left(\dfrac{\Gamma_1}{\Gamma_2}\right)$

Γ circulation (positive counterclockwise)

ρ mass density

Subscripts 1, 2, 3, and 4 refer to vortex number. (See sketch on page 5.)

GENERAL ANALYSIS

The phenomenon of the rolling up of the vortex sheet behind plane wings was discussed as early as 1907 by Lanchester (reference 3) and has since been the subject of a large number of investigations. As a result of such investigations, it has been found (reference 2) that, whereas the vortex sheet behind wings of high aspect ratio may be considered to remain flat at the tail location, a good approximation to the downwash several chord lengths behind wings of low aspect ratio is often obtained by considering the sheet to be fully rolled up into two trailing vortices. In the case of the cruciform wing, as in the case of the plane wing, the rate of rolling up of the vortex sheets will depend upon the aspect ratio of each wing. It should therefore be possible to obtain a reasonably good approximation to the downwash field behind low-aspect-ratio cruciform wings by considering the vortex sheets to be fully rolled up; that is, by replacing the two vortex sheets by four discrete vortices. It is with this simplified model of the physical problem that the analysis of this report is concerned at the outset. Subsequently, it will be seen that the theory can be modified to provide a more accurate representation of the actual flow field.

With low-aspect-ratio wings in source-free flow the linearized differential equation for the perturbation velocity potential φ

$$(1-M^2)\varphi_{xx} + \varphi_{yy} + \varphi_{zz} = 0 \tag{1}$$

can be satisfactorily approximated at all Mach numbers by the two-dimensional equation

$$\varphi_{yy} + \varphi_{zz} = 0 \tag{2}$$

since $(1-M^2)\,\varphi_{xx}$ is much smaller than φ_{yy} and φ_{zz} if $\sqrt{1-M^2}\,A$ is small. (See references 4 and 5.) Therefore, the problem of the motions of the four rolled-up vortices can first be treated by lateral strip theory as a two-dimensional problem in planes perpendicular to the flight direction. For the cruciform wing at 45° angle of bank, where a vertical plane of symmetry is present, the problem is thus reduced to that of the motion of two pairs of vortices with a common axis. This problem was first attacked by Love (reference 6) and later by Hicks (reference 7), both in connection with the analogous three-dimensional problem of the motion of vortex rings. Unfortunately, neither of these authors worked completely the problem of interest here, the former being concerned only with the relative paths of the vortex pairs about each other, whereas the latter was concerned chiefly with the actual problem of the vortex rings.

Since this paper is concerned with the three-dimensional paths of the four rolled-up vortices behind the wing, the paths in transverse planes will first be determined, and will then be related to the elapsed time or the distance the wing has traveled in the flight direction. The analysis will be confined to the case of 45° bank.

Determination of Vortex Paths

Relative motions in transverse plane.- The motion of any system of two-dimensional vortex filaments is determined by the induced velocity of each vortex due to all the other vortices of the system. It is shown in reference 8 that the induced velocity of any particular filament can be obtained from the function

$$W = \frac{i}{4\pi^2} \Sigma\Gamma_m\Gamma_n \log (\zeta_m - \zeta_n) \tag{3}$$

where $m < n$ and $\zeta_m = y_m + iz_m$. That is, if one writes

$$W = \Phi + i\psi \tag{4}$$

then ψ is a constant of the motion and is analogous to the stream function in giving the components of the velocity of the particular vortex. Thus, the path of each vortex can be determined from equations (3) and (4), provided that the motion of one vortex determines the motions of all the other vortices of the system. (Such is the case, for instance, where all the vortices but one are images of the one.) In the present problem, since only two of the four vortices are images, equations (3) and (4) are not sufficient to describe completely the motion of the system. However, these equations will be useful in determining the paths of two of the vortices relative to the other two. It will be seen later that this information is of considerable interest.

For the cruciform wing banked 45°, the simplified vortex system as viewed in the y,z plane consists of two pairs of two-dimensional vortices having a common plane of symmetry as shown in the sketch. It is apparent from the symmetry of the configuration that

$$\Gamma_1 = -\Gamma_4; \ \Gamma_2 = -\Gamma_3$$

Further, if each wing of the cruciform can be considered as a plane wing in sideslip (as was demonstrated in reference 9 for the calculation of load distribution) it follows that

$$\Gamma_1 = -\Gamma_3; \ \Gamma_2 = -\Gamma_4$$

since the vortex system far behind a plane lifting wing must consist of two equal (and opposite) vortices, although their positions will depend upon the angle of sideslip while their strength will depend upon the

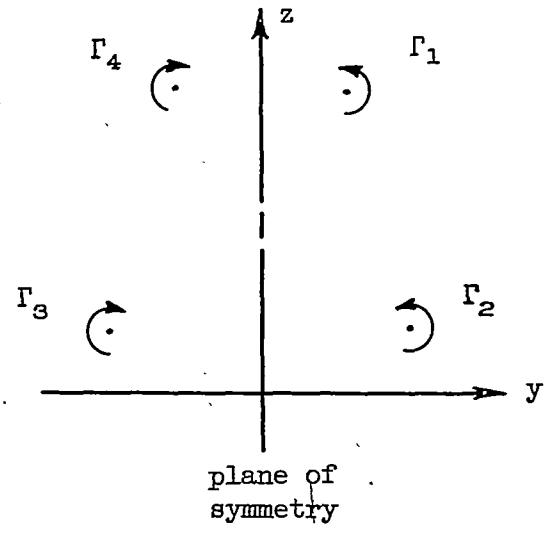

lift. On this basis, it can be concluded that

$$\Gamma_1 = \Gamma_2 = -\Gamma_3 = -\Gamma_4 = \Gamma$$

Actually, since the vortex sheets trailing behind the cruciform wing must influence one another during the rolling-up process itself, the assumption that the wings act independently is not strictly applicable to considerations of the wake as in the present problem. However, this complication will be deferred to a later section and the analysis will first be developed on the basis of four vortices of equal strength. Hence, from this point on, the subscripts will be omitted in reference to the vortex strengths which will be referred to simply as plus or minus Γ.

When the directions of rotation of the four vortices are taken into consideration, equation (3) can be written for the present problem as:

$$W = \frac{i\Gamma^2}{4\pi^2}\Big[\log(\zeta_1-\zeta_2) - \log(\zeta_2-\zeta_3) + \log(\zeta_3-\zeta_4) - \log(\zeta_1-\zeta_4) - \log(\zeta_1-\zeta_3) - \log(\zeta_2-\zeta_4)\Big] \quad (5)$$

Noting further that ζ_4 and ζ_3 are simply the negative complex conjugates of ζ_1 and ζ_2, that is $\zeta_4 = -\bar{\zeta}_1$, $\zeta_3 = -\bar{\zeta}_2$, equation (5) can be expressed as

$$W = \frac{i\Gamma^2}{4\pi^2}\Big[\log(\zeta_1-\zeta_2) - \log(\zeta_2 + \bar{\zeta}_2) + \log(\bar{\zeta}_1-\bar{\zeta}_2) - \log(\zeta_1 + \bar{\zeta}_1) - \log(\zeta_1 + \bar{\zeta}_2) - \log(\zeta_2 + \bar{\zeta}_1)\Big]$$

$$= \frac{i\Gamma^2}{4\pi^2}\log\left[\frac{(\zeta_1-\zeta_2)(\bar{\zeta}_1-\bar{\zeta}_2)}{(\zeta_2+\bar{\zeta}_2)(\zeta_1+\bar{\zeta}_1)(\zeta_1+\bar{\zeta}_2)(\zeta_2+\bar{\zeta}_1)}\right] \quad (6)$$

Due to the symmetry (see sketch on page 5), the vortex system may also be considered as two groups of vortices with equal and opposite total circulation (one group on either side of the plane of symmetry). For such a pair of groups, the centers of gravity[1] of the two groups must remain a fixed distance apart. (See reference 10.) In other words, the center of gravity of each group must move parallel to the plane of symmetry. Since here the strengths are equal in magnitude, this may be stated as

$$y_{c.g.} = \frac{\Sigma y_i\Gamma_i}{\Sigma\Gamma_i} = \frac{\Gamma(y_1+y_2)}{2\Gamma} = \frac{y_1+y_2}{2} \equiv \frac{f}{2} = \text{constant} \quad (7)$$

[1]The center of gravity of a group of vortices is defined as the center of gravity of a similar field of point masses, the mass of each being proportional to the strength of the corresponding vortex. Negative masses correspond to negative circulations.

With this information, equation (6) can be expressed in terms of the coordinates y and z and simplified to

$$W = \frac{i\Gamma^2}{4\pi^2} \log \left\{ \frac{(y_1-y_2)^2 + (z_1-z_2)^2}{4y_1y_2\,[f^2+(z_1-z_2)^2]} \right\} \tag{8}$$

Now, since W is purely imaginary, equation (4) is simply

$$\psi = \frac{\Gamma^2}{4\pi^2} \log \left\{ \frac{(y_1-y_2)^2 + (z_1-z_2)^2}{4y_1y_2[f^2+(z_1-z_2)^2]} \right\} \tag{9}$$

At this point, a moving coordinate system is introduced such that one pair of vortices always lies on the y axis. This is done by a change of variable

$$z_{1,2} = z_1 - z_2 \tag{10}$$

Now, noting that $y_2 = f - y_1$, equation (9) becomes

$$\psi = \frac{\Gamma^2}{4\pi^2} \log \left[\frac{(2y_1-f)^2 + z_{1,2}^2}{4y_1(f-y_1)(f^2+z_{1,2}^2)} \right] \tag{11}$$

Setting ψ of equation (11) equal to a constant then yields an equation for the paths of vortices 1 and 2 relative to each other. Thus,

$$\frac{(2y_1-f)^2 + z_{1,2}^2}{y_1(f-y_1)(f^2+z_{1,2}^2)} = \text{constant}$$

or

$$\frac{\left(2\frac{y_1}{f}-1\right)^2 + \left(\frac{z_{1,2}}{f}\right)^2}{\frac{y_1}{f}\left(1-\frac{y_1}{f}\right)\left[1+\left(\frac{z_{1,2}}{f}\right)^2\right]} = \text{constant} = G \tag{12}$$

determines the relative paths of vortices 1 and 2 (and also 3 and 4) once the value of the constant G is determined.

In order to evaluate G of equation (12), one must determine the initial positions of the four vortices. It must be realized, of course, that initially (i.e., at the trailing edges of the cruciform wings) there are not four discrete vortices but a cruciform system of vortex sheets. The immediate problem, then, is to replace these sheets by four vortices properly located in the ζ(or y,z) plane. For the present, it will suffice to observe that the initial locations of the four vortices must lie on the straight lines formed by the trailing edges of the wings.

Thus, for 45° bank,

$$z_{1,2} = y_1 + y_2 = f \text{ when } y_1 = y_o \tag{13}$$

where the subscript o refers to the initial value of y_1. The actual determination of y_o will be deferred to a later section of this report in which the physical problem will be considered in more detail.

With the boundary condition expressed in equation (13), equation (12) can be written in terms of the initial value of y_1:

$$\left(\frac{z_{1,2}}{f}\right)^2 = \frac{G\,\frac{y_1}{f}\left(1 - \frac{y_1}{f}\right) - \left(2\,\frac{y_1}{f} - 1\right)^2}{1 - G\,\frac{y_1}{f}\left(1 - \frac{y_1}{f}\right)} \tag{14}$$

where

$$G = \frac{\left(2\,\frac{y_o}{f} - 1\right)^2 + 1}{2\,\frac{y_o}{f}\left(1 - \frac{y_o}{f}\right)} = \frac{1}{\frac{y_o}{f}\left(1 - \frac{y_o}{f}\right)} - 2$$

It will be shown later that y_o, and hence G, is a function of angle of attack for the cruciform-wing configuration.

While equation (14) does not completely describe the motion of the four vortices, it yields some interesting information regarding the types of motion to be expected. For instance, if the relative path described by equation (14) is a closed curve it can be concluded that the motion is periodic. The relative paths of the vortices are plotted in figure 1 for various values of G, and it is found that the motion is periodic for G less than 4 and aperiodic for G greater than 4. This is in agreement with the findings of Love (reference 6) who showed that the condition for periodic motion is that

$$r < 3 + 2\sqrt{2} \tag{15}$$

where $r = \frac{y_2}{y_1}$ at $z_{1,2} = 0$. That is, r is the ratio of the lateral displacements from the plane of symmetry when the four vortices are collinear (when one pair is passing through the other). This type of vortex motion was first discussed by Helmholtz in connection with vortex rings having the same axis and circulations in the same direction (reference 11):

> "The foremost widens and travels more slowly, the pursuer shrinks and travels faster, till finally, if their velocities are not too different, it overtakes the first and penetrates it. Then the same game goes on in the opposite order, so that the rings pass through each other alternately."

Complete motions in transverse plane.- Since the relative paths of the vortices on either side of the plane of symmetry are given by equation (14), establishing the actual path of any one of the four vortices will completely determine the motion of the system in the y,z plane. Therefore, the actual path of vortex 1 will now be calculated.

The determination of any of the individual vortex paths requires the solution of the following equation:

$$z_n = \int \frac{dz_n}{dy_n}\, dy_n = \int \frac{dz_n/dt}{dy_n/dt}\, dy_n = \int \frac{w_n}{v_n}\, dy_n \tag{16}$$

where v_n and w_n are the velocity components of the nth vortex in the y and z directions, respectively. If equation (16) is evaluated for one vortex, say vortex 1, then the path of vortex 2 can be obtained from equations (7), (10), and (14), and the paths of vortices 3 and 4 are found by symmetry. It will be seen that this is considerably easier than solving four equations of the type given by equation (16). By adding the contributions of all the other vortices to the velocity components of vortex 1, one finds (see sketch):

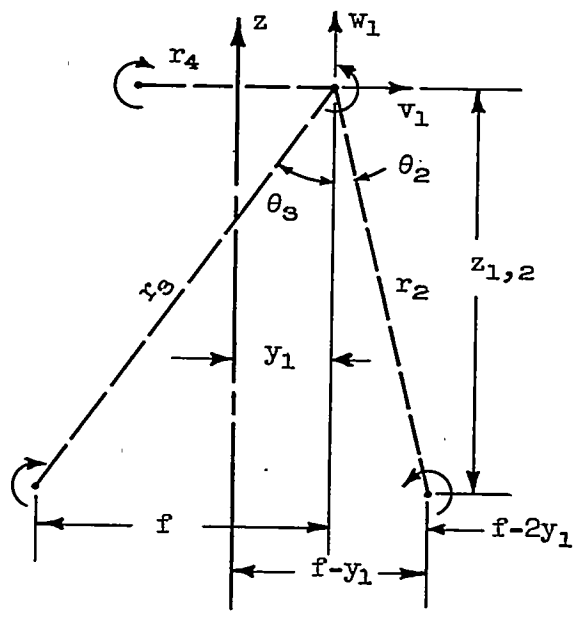

$$v_1 = -\frac{\Gamma}{2\pi r_2}\cos\theta_2 + \frac{\Gamma}{2\pi r_3}\cos\theta_3$$

and

$$w_1 = -\frac{\Gamma}{2\pi r_4} - \frac{\Gamma}{2\pi r_2}\sin\theta_2 - \frac{\Gamma}{2\pi r_3}\sin\theta_3 \tag{17}$$

Further, from the geometry of the system, it is seen that

$$\frac{\cos\theta_2}{r_2} = \frac{z_{1,2}}{z_{1,2}^2 + (f - 2y_1)^2}; \quad \frac{\cos\theta_3}{r_3} = \frac{z_{1,2}}{z_{1,2}^2 + f^2}$$

$$\frac{\sin\theta_2}{r_2} = \frac{f - 2y_1}{z_{1,2}^2 + (f - 2y_1)^2}; \quad \frac{\sin\theta_3}{r_3} = \frac{f}{z_{1,2}^2 + f^2}$$

and

$$r_4 = 2y_1$$

The velocity components v_1 and w_1 can now be expressed in the following form:

$$v_1 = -\frac{2\Gamma z_{1,2}}{\pi}\left\{\frac{y_1(f-y_1)}{[z_{1,2}^2 + (f-2y_1)^2][z_{1,2}^2 + f^2]}\right\}$$

$$w_1 = -\frac{\Gamma}{4\pi}\left\{\frac{(f^2 + z_{1,2}^2)^2 - 8fy_1^2\,(f - y_1)}{y_1(f^2 + z_{1,2}^2)[z_{1,2}^2 + (f - 2y_1)^2]}\right\} \tag{18}$$

If equations (14) and (18) are used to express v_1 and w_1 as functions of y_1, then equation (16) can be integrated directly to give the path of vortex 1. After algebraic manipulation, equation (16) thus becomes

$$z_1-z_0 = \int_{y_0}^{y_1} \frac{f^4+2f^3y_1(G-1)-Gf^2y_1^2(G+2)+2G^2fy_1^3-G^2y_1^4}{(f^2-Gfy_1+Gy_1^2)\sqrt{[-(G+4)y_1^2+f(G+4)y_1-f^2][Gy_1^2-Gfy_1+f^2]}}\,dy_1 \tag{19}$$

where z_0 is the initial value of z_1.

If now the numerator of the integrand is divided by the rational factor in the denominator, and the substitution

$$y_1 = \eta + \frac{f}{2}$$

is made, then the quantity $(z_1 - z_0)$ can be expressed as the sum of four integrals

$$z_1-z_0 = \frac{1}{\sqrt{G(G+4)}}\left[-G\int_{y_0-\frac{f}{2}}^{y_1-\frac{f}{2}} \frac{\eta^2 d\eta}{\sqrt{(R^2-\eta^2)(Q^2+\eta^2)}} - Q^2G\int_{y_0-\frac{f}{2}}^{y_1-\frac{f}{2}} \frac{d\eta}{\sqrt{(R^2-\eta^2)(Q^2+\eta^2)}} + \right.$$

$$\left.\frac{f^4}{G}\int_{y_0-\frac{f}{2}}^{y_1-\frac{f}{2}} \frac{d\eta}{(Q^2+\eta^2)\sqrt{(R^2-\eta^2)(Q^2+\eta^2)}} - \frac{2f^3}{G}\int_{y_0-\frac{f}{2}}^{y_1-\frac{f}{2}} \frac{\eta\, d\eta}{(Q^2+\eta^2)\sqrt{(R^2-\eta^2)(Q^2+\eta^2)}}\right] \tag{20}$$

where $R^2 \equiv \frac{f^2G}{4(G+4)}$ and $Q^2 \equiv \frac{f^2(4-G)}{4G}$.

Equation (20) is now in a convenient form if G is less than 4. This corresponds to the range for periodic motion. On the other hand, if G is greater than 4 (aperiodic), a new constant

$$\bar{Q}^2 = -Q^2 = \frac{f^2(G-4)}{4G}$$

is introduced so that equation (20) becomes

$$z_1-z_0 = \frac{1}{\sqrt{G(G+4)}}\left[-G\int_{y_0-\frac{f}{2}}^{y_1-\frac{f}{2}} \frac{\eta^2 d\eta}{\sqrt{(R^2-\eta^2)(\eta^2-\bar{Q}^2)}} + \bar{Q}^2 G\int_{y_0-\frac{f}{2}}^{y_1-\frac{f}{2}} \frac{d\eta}{\sqrt{(R^2-\eta^2)(\eta^2-\bar{Q}^2)}} + \right.$$

$$\left.\frac{f^4}{G}\int_{y_0-\frac{f}{2}}^{y_1-\frac{f}{2}} \frac{d\eta}{(\eta^2-\bar{Q}^2)\sqrt{(R^2-\eta^2)(\eta^2-\bar{Q}^2)}} - \frac{2f^3}{G}\int_{y_0-\frac{f}{2}}^{y_1-\frac{f}{2}} \frac{\eta\, d\eta}{(\eta^2-\bar{Q}^2)\sqrt{(R^2-\eta^2)(\eta^2-\bar{Q}^2)}}\right] \tag{21}$$

The third possibility is that G is equal to 4, in which case $Q^2 = \bar{Q}^2 = 0$. Equations (20) and (21) then both reduce to

$$z_1-z_0 = -\frac{1}{\sqrt{2}}\int_{y_0-\frac{f}{2}}^{y_1-\frac{f}{2}} \frac{\eta\, d\eta}{\sqrt{R^2-\eta^2}} + \frac{f^4}{16\sqrt{2}}\int_{y_0-\frac{f}{2}}^{y_1-\frac{f}{2}} \frac{d\eta}{\eta^3\sqrt{R^2-\eta^2}} - \frac{f^3}{8\sqrt{2}}\int_{y_0-\frac{f}{2}}^{y_1-\frac{f}{2}} \frac{d\eta}{\eta^2\sqrt{R^2-\eta^2}} \tag{22}$$

The three cases corresponding to equations (20), (21), and (22) will be treated separately since the integrations will be somewhat different for each.

For cases where the vortex motion is periodic, that is, when G is less than 4, the determination of the vortex paths requires the evaluation of the integrals of equation (20). It is seen that the fourth integral of this equation is elementary while the first three are elliptic. Thus, while the fourth integral can be evaluated simply by noting that $\eta\, d\eta = \frac{1}{2}\, d(\eta^2)$, the other integrals require the use of the elliptic transformations[2]

[2]These and subsequent transformations were obtained from a comprehensive table of elliptic integrals prepared by Paul Byrd, Ames Laboratory, NACA.

$$\mathrm{sn}^2\, u_1 = \sin^2 \varphi_1 = \frac{R^2 - \left(y_1 - \frac{f}{2}\right)^2}{R^2}$$

$$\mathrm{sn}^2\, u_o = \sin^2 \varphi_o = \frac{R^2 - \left(y_o - \frac{f}{2}\right)^2}{R^2}$$

$$k^2 = \frac{R^2}{R^2 + Q^2} = \frac{G^2}{16} \tag{23}$$

With these transformations the integrals can be evaluated and the results expressed in terms of elliptic integrals of the first and second kinds. The final solution of equation (20), after collection of terms and evaluation of the constants, is given in nondimensional form by the expression

$$\frac{z_1}{f} = \frac{4G}{16-G^2}\left[E(k,\varphi_o) - E(k,\varphi_1)\right] + \frac{G^2}{8(4-G)}\left(\frac{\sin\varphi_1 \cos\varphi_1}{\sqrt{1-k^2\sin^2\varphi_1}} - \frac{\sin\varphi_o\cos\varphi_o}{\sqrt{1-k^2\sin^2\varphi_o}}\right) +$$

$$\frac{1}{8}\sqrt{G(G+4)}\left(\frac{\sin\varphi_1}{\sqrt{1-k^2\sin^2\varphi_1}} - \frac{\sin\varphi_o}{\sqrt{1-k^2\sin^2\varphi_o}}\right) + \frac{y_o}{f} \tag{24}$$

where $k = \frac{G}{4}$ and it is recalled that z_o is equal to y_o due to the 45° configuration of the initial locations of the vortices. (Note that φ_o lies in the second quadrant and that φ_1 increases positively from φ_o.) Thus, for the case where the motion is periodic, the motion in the y,z plane is completely described by equations (7), (10), (14) and (24).

If the motion in the y,z plane is not periodic, that is, if G is greater than 4, then the motion of vortex 1 is described by equation (21). Here again the first three integrals of this equation are elliptic, but now the required transformations are

$$\mathrm{sn}^2\, u_1 = \sin^2 \varphi_1 = \frac{R^2 - \left(y_1 - \frac{f}{2}\right)^2}{R^2 - \bar{Q}^2}$$

$$\mathrm{sn}^2\, u_o = \sin^2 \varphi_o = \frac{R^2 - \left(y_o - \frac{f}{2}\right)^2}{R^2 - \bar{Q}^2}$$

$$k^2 = \frac{R^2 - \bar{Q}^2}{R^2} = \frac{16}{G^2} \tag{25}$$

It should be noted that for this case (aperiodic motion) when η^2 is less than $\bar{Q}^2$, all four integrals become imaginary. That is, z_1 is imaginary if

$$\left|\frac{y_1}{f} - \frac{1}{2}\right| < \frac{\bar{Q}}{f} \tag{26}$$

This condition defines the asymptotes of the vortex paths for the aperiodic motion. This can be seen from the relative paths shown in figure 1.

If the integrals of equation (21) are now evaluated for this case, the resulting expression for the aperiodic path of vortex 1 is

$$\frac{z_1}{f} = -\frac{G^2}{G^2-16}\left[E(k,\varphi_o) - E(k,\varphi_1)\right] + F(k,\varphi_o) - F(k,\varphi_1) +$$

$$\frac{G}{2(G-4)}\left(\tan\varphi_o\sqrt{1-k^2\sin^2\varphi_o} - \tan\varphi_1\sqrt{1-k^2\sin^2\varphi_1}\right) +$$

$$\frac{1}{2}\sqrt{\frac{G+4}{G}}\left(\tan\varphi_o - \tan\varphi_1\right) + \frac{y_o}{f} \tag{27}$$

where $k = \frac{4}{G}$. The motion is now completely defined by equations (7), (10), (14), and (27).

For the special case when G is equal to 4, all the integrals are elementary and can readily be evaluated by making use of the trigonometric substitutions

$$\cos\varphi_1 = \frac{y_1 - \frac{f}{2}}{R}; \quad \cos\varphi_o = \frac{y_o - \frac{f}{2}}{R} \tag{28}$$

The final solution of equation (22) is then

$$\frac{z_1}{f} = -\frac{1}{4}\left(\sin\varphi_1 - \sin\varphi_o\right) + \frac{1}{2}\left(\frac{\sin\varphi_1}{\cos^2\varphi_1} - \frac{\sin\varphi_o}{\cos^2\varphi_o}\right) +$$

$$\frac{1}{2}\log\frac{\cos\varphi_o(1+\sin\varphi_1)}{\cos\varphi_1(1+\sin\varphi_o)} - \frac{1}{\sqrt{2}}\left(\frac{\sin\varphi_1}{\cos\varphi_1} - \frac{\sin\varphi_o}{\cos\varphi_o}\right) +$$

$$\frac{1}{2}\left(1 - \frac{1}{\sqrt{3}}\right) \tag{29}$$

Actually, it can be shown that this result is obtainable from either equation (24) or (27) by taking the limit as G approaches 4. It is interesting to note that G can assume only positive values and must lie between 2 and infinity as can be seen from its definition given with equation (14). Thus, the vortex paths in the y,z plane have been obtained for the entire range of the parameter G. Figure 2 shows the paths of vortices 1 and 2 for several values of G. The dashed lines connect corresponding positions of the two vortices at successive time intervals.

Complete motions in three dimensions.- In order to complete the three-dimensional picture of the four vortex filaments trailing behind the cruciform wings, a relationship must be obtained between the points of the paths in the y,z plane and the distance the wing has traveled in the stream direction. This can be done by the relationship

$$d = Ut = U\int dt = U\int \frac{dy_1}{dy_1/dt} = U\int \frac{dy_1}{v_1} \tag{30}$$

Equations (14) and (18) can again be used to express v_1 as a function of y_1 so that equation (30) can be integrated. The integral thus becomes

$$d = -\frac{8\pi GfU}{\Gamma}\int_{y_0}^{y_1} \sqrt{\frac{f^2-Gy_1(f-y_1)}{Gy_1(f-y_1)-(2y_1-f)^2}} \left\{\frac{y_1^2(f-y_1)^2}{[f^2-Gy_1(f-y_1)]^2}\right\} dy_1 \tag{31}$$

Again using the substitution

$$y_1 = \eta + \frac{f}{2}$$

equation (31) can be simplified into three somewhat different forms, one for each of the three regimes of the parameter G.

For the case when G is less than 4 (periodic motion), equation (31) can be written as

$$d = -\frac{8\pi fU}{\Gamma\sqrt{G(G+4)}}\int_{y_0-\frac{f}{2}}^{y_1-\frac{f}{2}} \frac{\left(\frac{f^2}{4}-\eta^2\right)^2 d\eta}{(Q^2+\eta^2)\sqrt{(R^2-\eta^2)(Q^2+\eta^2)}} \tag{32}$$

where

$$R^2 = \frac{f^2G}{4(G+4)} \text{ and } Q^2 = \frac{f^2(4-G)}{4G}$$

For the aperiodic case (G greater than 4), equation (31) becomes

$$d = -\frac{8\pi fU}{\Gamma\sqrt{G(G+4)}}\int_{y_o-\frac{f}{2}}^{y_1-\frac{f}{2}} \frac{\left(\frac{f^2}{4}-\eta^2\right)^2 d\eta}{(\eta^2-\bar{Q}^2)\sqrt{(R^2-\eta^2)(\eta^2-\bar{Q}^2)}} \tag{33}$$

where

$$\bar{Q}^2 = -Q^2 = \frac{f^2(G-4)}{4G}$$

while for the special case when G is equal to 4, equations (32) and (33) both reduce to

$$d = -\frac{8\pi fU}{\Gamma\sqrt{G(G+4)}}\int_{y_o-\frac{f}{2}}^{y_1-\frac{f}{2}} \frac{\left(\frac{f^2}{4}-\eta^2\right)^2 d\eta}{\eta^3\sqrt{R^2-\eta^2}} \tag{34}$$

since here $Q^2 = \bar{Q}^2 = 0$.

The three expressions for the distance behind the wing can now be solved by use of the proper elliptic transformations. For G less than 4, the result is

$$\frac{d}{f} = \frac{\pi Uf}{\Gamma}\left\{-\frac{128}{G(16-G^2)}\left[E(k,\varphi_o)-E(k,\varphi_1)\right] + \frac{8}{G}\left[F(k,\varphi_o)-F(k,\varphi_1)\right] + \frac{G}{4-G}\left(\frac{\sin\varphi_o\cos\varphi_o}{\sqrt{1-k^2\sin^2\varphi_o}} - \frac{\sin\varphi_1\cos\varphi_1}{\sqrt{1-k^2\sin^2\varphi_1}}\right)\right\} \tag{35}$$

where

$$k^2 = \frac{R^2}{R^2+Q^2} = \frac{G^2}{16},\quad \sin^2\varphi_1 = \frac{R^2-\left(y_1-\frac{f}{2}\right)^2}{R^2},\quad \text{and } \sin^2\varphi_o = \frac{R^2-\left(y_o-\frac{f}{2}\right)^2}{R^2}$$

For G greater than 4, the resulting expression is

$$\frac{d}{f} = \frac{\pi U f}{\Gamma} \left\{ \frac{32}{G^2-16} \left[E(k,\varphi_o)-E(k,\varphi_1) \right] - \right.$$

$$\left. \frac{4}{G-4} \left(\tan \varphi_o \sqrt{1-k^2 \sin^2 \varphi_o} - \tan \varphi_1 \sqrt{1-k^2 \sin^2 \varphi_1} \right) \right\} \tag{36}$$

where

$$k^2 = \frac{R^2-\bar{Q}^2}{R^2} = \frac{16}{G^2}, \quad \sin^2 \varphi_1 = \frac{R^2-\left(y_1-\frac{f}{2}\right)^2}{R^2-\bar{Q}^2}, \text{ and } \sin^2 \varphi_o = \frac{R^2-\left(y_o-\frac{f}{2}\right)^2}{R^2-\bar{Q}^2}$$

For G equal to 4,

$$\frac{d}{f} = \frac{\pi U f}{\Gamma} \left[\frac{\sin \varphi_o}{\cos^2 \varphi_o} - \frac{\sin \varphi_1}{\cos^2 \varphi_1} + \log \frac{(1+\sin \varphi_1)(-\cos \varphi_o)}{(1+\sin \varphi_o)(-\cos \varphi_1)} + \frac{1}{2} (\sin \varphi_o - \sin \varphi_1) \right] \tag{37}$$

where

$$\cos^2 \varphi_1 = \frac{\left(y_1-\frac{f}{2}\right)^2}{R^2} \text{ and } \cos^2 \varphi_o = \frac{\left(y_o-\frac{f}{2}\right)^2}{R^2}$$

With the aid of equations (35), (36), and (37), the positions of the four rolled-up vortices are completely described[3] for all distances behind the cruciform wings. Thus, for G less than 4, equations (7), (10), (14), (24), and (35) completely determine the motion. The other cases are given by the corresponding equations.

APPLICATION TO CRUCIFORM TRIANGULAR WING AT 45° BANK

Determination of Initial Vortex Positions and Vortex Strengths

The equations thus far developed give the motions of the rolled-up vortices in terms of their initial positions. In order to relate these motions to physical cases involving a given cruciform wing at a specified angle of attack, the initial positions of the four vortices must be determined as a function of the lift coefficient. This amounts

[3]The evaluation of the circulation Γ will be discussed in the next section.

to the determination of the parameter G in terms of the physical quantities such as lift coefficient and aspect ratio. Therefore, this section will be concerned with the initial locations of the four vortices for a given cruciform wing (banked 45°) at a given flight condition.

Since the vortices trailing behind the cruciform wing actually leave the trailing edges as two flat vortex sheets, the initial locations of the four rolled-up vortices are somewhat fictitious. However, if each wing of the cruciform is considered as a plane wing in sideslip, the locations of the rolled-up vortices from each wing can be calculated from the span loading curve. Such a calculation, then, can be considered as yielding the positions of the four vortices of the cruciform before any interaction has taken place between the vortices of the two wings, namely, immediately behind the trailing edges. Hence, in order to calculate the initial positions of the four vortices, the span loadings of the separate wings must be determined.

In reference 9, it was shown that the load distribution on each wing of a pointed low-aspect-ratio cruciform wing with no body is given by the expression

$$\left(\frac{\Delta p}{q}\right) = \frac{4\alpha'\left(\frac{ds}{dx} + \beta\,\frac{y}{s}\right)}{\sqrt{1 - \frac{y^2}{s^2}}} \tag{38}$$

where Δp is the difference in pressure between corresponding points on the upper and lower surfaces of the individual wing.

Equation (38) is not valid for angles of sideslip greater than $\frac{ds}{dx}$. The span loading is obtained by integrating this load distribution in the chordwise direction; that is

$$\begin{aligned} c_l c &= \int_{L.E.}^{T.E.} \left(\frac{\Delta p}{q}\right) dx \\ &= \int_{\frac{y}{ds/dx}}^{\frac{s_o}{ds/dx}} \frac{4\alpha'\left(\frac{ds}{dx} + \beta\,\frac{y}{s}\right)}{\sqrt{1 - \frac{y^2}{s^2}}}\, dx \end{aligned} \tag{39}$$

Equation (39) can be separated into two integrals, and since for triangular wings ds/dx is a constant, the resulting span loading is

$$c_l c = 4\alpha' s_o \left(\sqrt{1 - \frac{y^2}{s_o^2}} + \frac{\beta}{ds/dx} \frac{y}{s_o} \log \frac{1 + \sqrt{1-y^2/s_o^2}}{|y/s_o|}\right) \tag{40}$$

or, since $ds/dx = \frac{A}{4}$ for triangular wings,

$$c_l c = 4\alpha' s_o \left(\sqrt{1 - \frac{y^2}{s_o^2}} + \frac{4\beta}{A} \frac{y}{s_o} \log \frac{1 + \sqrt{1-y^2/s_o^2}}{|y/s_o|}\right) \tag{41}$$

In the case of the unyawed plane wing, it is clear from symmetry considerations that, if the vortex sheet is to roll up into two vortices, all the vorticity on one side of the plane of symmetry must eventually become rolled up into one vortex. This leads to the conclusion that each rolled-up vortex must be of strength equal to the maximum circulation which in this case is the circulation in the plane of symmetry. A corollary of this conclusion is that each rolled-up vortex contains only vortices of the same sense. This seems to be in accordance with existing knowledge of the behavior of vortex sheets as well as with existing theories of the cumulation of vorticity as applied to turbulence. For the wing in sideslip, whereas there is no symmetry, the wing can again be considered as composed of two segments, each having vorticity in only one direction and hence each producing one rolled-up vortex. The dividing line between two such segments is at the spanwise station of maximum circulation so that such a division leads to the conclusion that each rolled-up vortex must have a strength equal to the maximum circulation. Thus, the vortex strength is given by

$$\Gamma = \frac{U}{2} (c_l c)_{max} \tag{42}$$

Further, the distance between the vortices is given by the fact that the lift impulse must always be that of the wing itself. Thus,

$$2s' = \frac{L'}{\rho U \Gamma} = \frac{C_L' S}{(c_l c)_{max}} \tag{43}$$

From equation (43) it can be seen that the distance $2s'$ can be represented on the span loading curve as shown in the sketch, where the area under the rectangle is equal to the area under the curve.

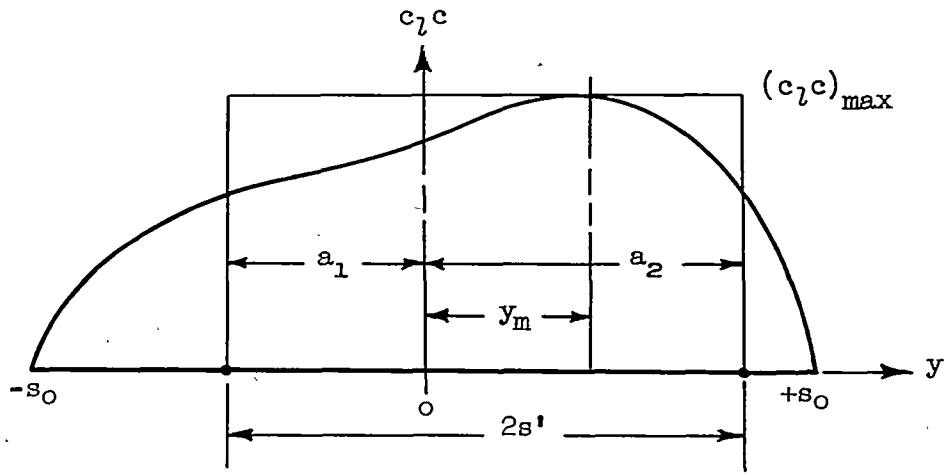

As seen from the sketch, the actual location of each of the vortices still requires the determination of the distances a_1 and a_2. It has already been argued that all the vorticity on one side of the maximum circulation must eventually be contained in one rolled-up vortex. Thus the two areas can be equated on either side of the maximum; that is,

$$(a_1 + y_m)(c_l c)_{max} = \int_{-s_o}^{y_m} c_l c \, dy$$

$$(a_2 - y_m)(c_l c)_{max} = \int_{y_m}^{+s_o} c_l c \, dy \tag{44}$$

(Note that y_m is readily calculated by successive approximations.)

To apply the above information to the cruciform wing at 45° bank, one merely needs to note that for this case

$$\alpha' = \beta = \alpha \sin 45^\circ = \frac{\alpha}{\sqrt{2}}$$

and that the initial position of vortex number 1 in the banked coordinate system is now given by $y_o = \frac{a_1}{\sqrt{2}}$. It is further pointed out that

$$f = y_1 + y_2 = \frac{a_1 + a_2}{\sqrt{2}}$$

Since the lift of the cruciform wing can now be expressed as

$$L = \sqrt{2}\,\rho U\Gamma\,(a_1 + a_2) = \frac{1}{2}\,\rho U^2\,C_L\,S \tag{45}$$

and the wing area S is equal to $4s_o^2/A$, it is seen that the circulation Γ is given by

$$\frac{\Gamma}{U} = \frac{\sqrt{2}\,s_o^2}{a_1 + a_2}\left(\frac{C_L}{A}\right) \tag{46}$$

Sufficient information is now at hand to determine the initial positions of the four vortices as a function of the angle of attack for a particular aspect ratio or, more generally, as a function of α/A. However, since the above span loadings were obtained from low-aspect-ratio theory, for which $C_L = \frac{\pi}{2}A\alpha$, the results can be considered as a function of the parameter $C_L/\pi A^2$. It can be shown that this will make the results more general in that they will now apply with the accuracy of linearized theory rather than of low-aspect-ratio theory. This may be seen from the fact that the loadings in linearized theory (see, e.g., reference 12) for triangular wings are simply those of low-aspect-ratio theory multiplied by a constant which depends upon the aspect ratio and the Mach number.

The theoretical initial positions of vortex 1 have been calculated and are plotted against $C_L/\pi A^2$ in figure 3. From these initial positions, the values of G were calculated (equation (14)), and are plotted in figure 4. The limiting angle of sideslip of equations (38) and (41) has been exceeded somewhat, as indicated by the dashed portion of the curve in figure 3, in order to permit some interesting observations regarding the indicated trends. The constants appearing in the equations for the vortex paths have now been completely determined and the three-dimensional paths of the four vortices can be calculated for any lift coefficient and aspect ratio. An illustration of such paths for a typical case is presented in figure 5.

If one recalls the types of motion associated with the various regimes of G, figure 3 takes on added significance. The passing from periodic motion to aperiodic motion simply indicates the inward movement of the initial position of the upper two vortices with angle of attack until their velocity in the z direction is so great that once they pass through the lower vortices, the latter never catch up to complete the cycle. If this inward movement were to continue as the angle of attack increases (as shown in fig. 3) then at $C_L/\pi A^2 = 0.244$ the two upper vortices would have coalesced, leaving only the two lower vortices which would then travel parallel to the z axis as in the case of a plane wing.

Leapfrog Distance

As an indication of the practical importance of the motion of the four rolled-up vortices in the calculation of downwash, a distance behind the wing which is characteristic of the motion will be calculated. This distance is taken as the distance at which the four vortices have become collinear, that is, the distance behind the wing at which the upper two vortices are just passing through the lower two. This will be referred to as the leapfrog distance d_L measured from the wing trailing edges.

The leapfrog distance can be calculated directly from equation (31) by taking the upper limit of integration to be the value of y_1 in the collinear configuration. This value of y_1 is obtained from equation (14) by setting $z_{1,2}$ equal to zero. Solution of this equation then gives the limit of integration y_1 as a function of G only and therefore of $C_L/\pi A^2$. The definite integral of equation (31) has been evaluated by the methods discussed previously for the entire range of G and the resulting leapfrog distances are plotted (in terms of chord lengths) against $C_L/\pi A^2$ in figure 6. For purposes of comparison, as well as to provide a measure of the usefulness of the assumption that the four vortices are fully rolled up at the trailing edge, the distance for the vortex sheets to roll up (as calculated by Kaden, reference 1) is also shown in this figure. Since the distance to roll up as shown in figure 6 is that for a plane wing, it should be taken as an indication of the average distance for the four vortex sheets to roll up. Actually, because of the asymmetric span loading, the lower vortices will roll up somewhat faster, while those from the upper wing panels will roll up more slowly.

The outstanding point to be noted from figure 6 is that the phenomenon of leapfrogging can occur within a few chord lengths at reasonable lift coefficients for low-aspect-ratio triangular cruciform wings. The calculations are expected to represent the physical phenomenon most accurately when the leapfrog distance is considerably greater than the distance for the vortex sheets to roll up. The curves presented in figure 6 have been terminated at a value of $C_L/\pi A^2$ of 0.176, since above that value (calculated from low-aspect-ratio theory) the upper leading edges of the cruciform wing become trailing edges and the span load distributions are no longer given by equation (41).

Rolling Up of the Vortex Sheets

As was mentioned at the outset of the analysis, the assumption that the wings of the cruciform act independently of one another is not strictly applicable to the present problem because once the bound vortices of the wings become free (i.e., immediately behind the trailing

edge) the two vortex sheets influence one another in their subsequent behavior. Thus, while the foregoing analysis has treated in some detail the complete motions of the fully rolled-up vortices, it has not considered the mutual effects of the vortex sheets during the rolling-up process itself. Although a complete knowledge of the rolling-up process could be gained only by a detailed numerical analysis, some important questions regarding the over-all interaction effects can be answered by examining the nature of the vortex sheets in their initial cruciform configuration. Illustrated schematically in the sketch is the initial vortex configuration, showing the span loading or circulation distribution, which is the same on each wing, and the resulting vorticity with directions of rotation indicated by the arrows. In view of the arguments presented earlier, it is clear from the sketch that all the vortices contained in the distance AO will roll up into a single vortex, and that all those in BC will roll up into another single vortex with opposite direction of rotation. Furthermore, the strength of the latter vortex must clearly be equal to the maximum circulation Γ_{max}.

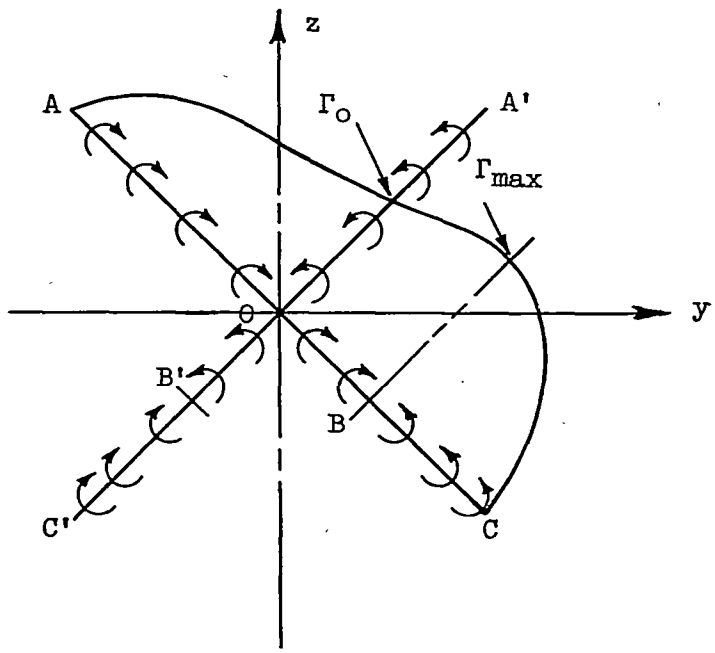

On the other hand, it is not clear just what will become of the vorticity contained in OB. If the wings did, in fact, act independently, then OB would certainly be combined with AO to form a single vortex of strength Γ_{max}. However, the presence of a plane of symmetry at $y = 0$ requires that AO and OB now be considered as separate vortex sheets since the vorticity at O vanishes due to symmetry. In fact, closer examination of the portion of the sheets near O reveals that, due to the directions of rotation, the broken-line sheet AOB' must move away from the sheet A'OB, thus severing AB and A'B' at O. It is doubtful, then, that the vorticity originally contained in OB and OB' will ever become entrained as a part of the upper two vortices. It will, in fact, later be shown, from the experiments conducted for this report, that this amount of vorticity actually forms

a separate sheet which is not identified as part of any of the four vortices treated thus far.

The foregoing observations suggest a possible improvement on the four-vortex analysis already carried out; that is, the strengths and initial positions of vortices 1 and 4 could be modified to take into account the fact that the vorticity in OB and OB' actually is not contained in vortices 1 and 4. The amount of vorticity in OB (hereafter referred to as Γ_c) and the resulting modification of Γ_1 is readily calculated from the span load distribution, as shown in the sketch. The strengths of the three vortices shown are simply given by

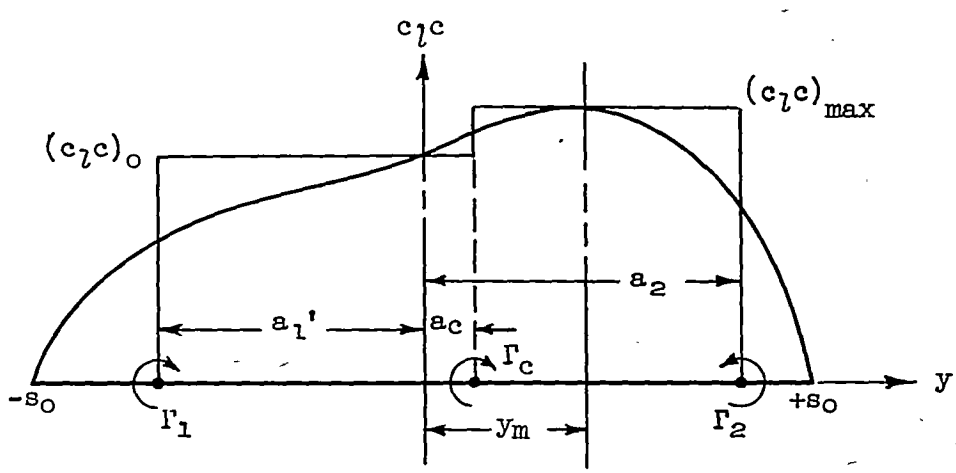

$$\Gamma_1 = \frac{U}{2}(c_l c)_o; \; \Gamma_2 = \frac{U}{2}(c_l c)_{max}$$

and

$$\Gamma_c = \Gamma_2 - \Gamma_1 = \frac{U}{2}\left[(c_l c)_{max} - (c_l c)_o\right] \tag{47}$$

The initial positions of the vortices are again calculated by equating the lift impulse before and after rolling up, but now Γ_1 is considered to contain only the vorticity arising from its side of the wing; that is,

$$a_1'(c_l c)_o = \int_{-s_o}^{o} c_l c \, dy$$

$$a_c(c_l c)_o + (y_m - a_c)(c_l c)_{max} = \int_{o}^{y_m} c_l c \, dy$$

$$(a_2 - y_m)(c_l c)_{max} = \int_{y_m}^{+s_o} c_l c \, dy \tag{48}$$

Note that a_2 is unchanged by the introduction of Γ_c.

With the aid of the foregoing sketch, one can again express the cruciform-wing lift in terms of the initial vortex positions

$$L = \sqrt{2}\ \rho U \left[\Gamma_1 (a_1' + a_c) + \Gamma_2 (a_2 - a_c)\right] = \frac{1}{2} \rho U^2 C_L S \qquad (49)$$

and conclude that

$$\frac{\Gamma_2}{U} = \frac{\sqrt{2}\, s_o^2}{[\gamma(a_1' + a_c) + a_2 - a_c]} \left(\frac{C_L}{A}\right) \qquad (50)$$

where

$$\gamma = \frac{\Gamma_1}{\Gamma_2}$$

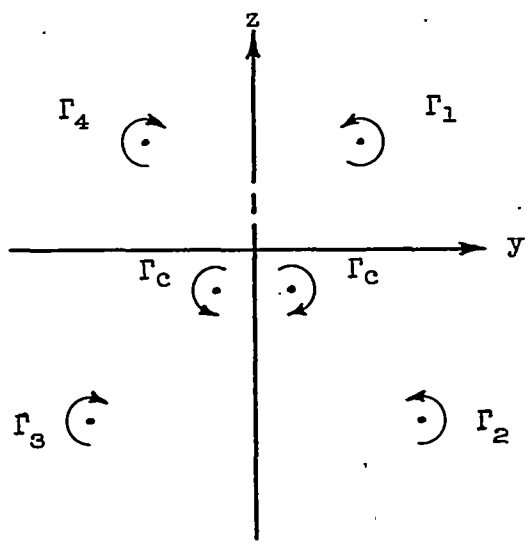

The original four-vortex problem has actually now been replaced by the six-vortex problem illustrated in the sketch. However, due to the relatively small strength of Γ_c, as well as to the close proximity of the two opposing vortices Γ_c, the influence of these additional vortices on the motions of the other four is expected to be small. An iterative approach to the exact solution can be obtained by neglecting this influence once the initial position and strength of Γ_1 have been modified to allow for Γ_c. Thus the problem is again simplified to that of the motion of four vortices, but now they have unequal strengths. (The ratio of the strengths Γ_1 to Γ_2 is plotted against $C_L/\pi A^2$ in fig. 7.) This fact alone complicates the mathematics to the point that the integrations can no longer be carried out except by numerical methods. Therefore, the complete motions will not be determined, but the leapfrog distance will be recalculated in order to illustrate the effect of the new assumptions on the results. The leapfrog distance is readily checked experimentally, as will be shown in the experimental section.

Modified Four-Vortex Calculation

The equations for the relative motion of the four vortices can again be set up by the use of the general equations (3) and (4) with a new statement of the center-of-gravity rule in which the vortex strengths are no longer taken to be equal. That is,

$$y_{c.g.} = \frac{\Sigma y_i \Gamma_i}{\Sigma \Gamma_i} = \frac{\Gamma_1 y_1 + \Gamma_2 y_2}{\Gamma_1 + \Gamma_2} = e = \text{constant} \tag{51}$$

If it is noted that in the initial configuration

$$z_{1,2} = y_1 + y_2;\ y_1 = y_0;\ y_2 = e\,(1 + \gamma) - \gamma y_0 \tag{52}$$

then equations (3) and (4) can be used as in the original analysis, resulting in the following expression (in dimensionless form) for the relative vortex paths:

$$\left(\frac{z_{1,2}}{e}\right)^2 = \frac{K\left[\frac{y_1}{e}(1-\gamma)+1+\gamma\right]^2 \left(\frac{y_1}{e}\right)^{\gamma}\left(1+\gamma-\gamma\frac{y_1}{e}\right)^{\frac{1}{\gamma}} - \left[\left(\frac{y_1}{e}-1\right)\left(1+\gamma\right)\right]^2}{1 - K\left(\frac{y_1}{e}\right)^{\gamma}\left(1+\gamma-\gamma\frac{y_1}{e}\right)^{\frac{1}{\gamma}}} \tag{53}$$

where

$$K \equiv \frac{\left(a_1'^2 + a_2^2\right)\left(\gamma + \frac{a_2}{a_1'}\right)^{\gamma}\left(\gamma\frac{a_1'}{a_2}+1\right)^{\frac{1}{\gamma}}}{\left(a_1' + a_2\right)^2\left(1+\gamma\right)^{\gamma+\frac{1}{\gamma}}}$$

The velocity v_1 is recalculated in the same manner as before, with the result

$$v_1 = \frac{2\Gamma_2}{\pi e}\left(\frac{z_{1,2}}{e}\right) \times$$

$$\left[\frac{\gamma\left(\frac{y_1}{e}\right)^2 - \left(1+\gamma\right)\frac{y_1}{e}}{\left\{\left(\frac{z_{1,2}}{e}\right)^2 + \left[\frac{y_1}{e}\left(1-\gamma\right)+1+\gamma\right]^2\right\}\left\{\left(\frac{z_{1,2}}{e}\right)^2 + \left[\left(\frac{y_1}{e}-1\right)\left(1+\gamma\right)\right]^2\right\}}\right] \tag{54}$$

If this expression is now used in equation (30) to determine the downstream distance d, the resulting (dimensionless) form of the integral is

$$\frac{d}{e} = \frac{\pi U e}{2\Gamma_2} \times$$

$$\int_{\frac{y_0}{e}}^{\frac{y_1}{e}} \left[\frac{\left\{\left(\frac{z_{1,2}}{e}\right)^2 + \left[\frac{y_1}{e}\left(1-\gamma\right)+1+\gamma\right]^2\right\}\left\{\left(\frac{z_{1,2}}{e}\right)^2 + \left[\left(\frac{y_1}{e}-1\right)\left(1+\gamma\right)\right]^2\right\}}{\left(\frac{z_{1,2}}{e}\right)\left[\gamma\left(\frac{y_1}{e}\right)^2 - \left(1+\gamma\right)\frac{y_1}{e}\right]}\right] d\left(\frac{y_1}{e}\right) \tag{55}$$

It is readily seen, without substituting the expression for $z_{1,2}/e$ as given by equation (53), that analytical evaluation of the integral of equation (55) would be extremely difficult. This integration was carried out numerically with the definite upper limit as given by the collinear configuration of the four vortices (i.e., $z_{1,2} = 0$) and the resulting values of the leapfrog distance d_L are plotted on figure 6. It is noted that the resulting curve is higher than that calculated in the original analysis. This is due primarily to the smaller strengths of the upper two vortices and to the consequently longer time required for them to pass through the lower two because of reduced induced velocities of one upon the other.

WATER-TANK EXPERIMENTS

The motions of the vortex sheets behind a triangular cruciform wing of aspect ratio 2 were observed experimentally by means of a water tank (fig. 8). The model was mounted on a vertical track which was driven at uniform speed into the tank, while photographs of the

water surface were recorded by a motion picture camera. The traces of the vortex sheets were made visible by applying fine aluminum powder to the trailing edges of the model. The model had a span of 8 inches and was made of 0.050-inch sheet metal.

In general, the purpose of the water-tank studies was simply to illustrate the motions analyzed in the earlier portions of this report. (A typical series of photographs enlarged from the moving pictures is presented in fig. 9.) However, it was a simple matter to obtain experimental values of the leapfrog distance by means of a tape which moved with the model track and recorded on the movie film the distance traveled by the wing. The results of such experiments are presented in figure 6 for several angles of attack and it is observed that the agreement with the modified four-vortex calculation is remarkably good.

The formation of a separate vortex sheet arising from the center portion of the cruciform wing, as discussed in a previous section, can be seen in the photographs of figure 9. This is the phenomenon that has been taken into account in the modified theory.

It is interesting to note (fig.9) that the two lower vortices extend downstream in nearly the free-stream direction as indicated by their positions relative to the wing-tip markers. This was also true for the calculated paths of figure 5.

An important feature of the actual flow field as distinguished from the simplified model used for the analysis is the persistence of the vortex sheets between the rolled-up vortices as seen in figure 9. Because of this fact, the theoretical paths of the vortices are not expected to be accurate at distances behind the wing greater than d_L, since vortices 1 and 4 will then begin to become entrained in the outer windings of the sheet that constitutes vortices 2 and 3. However, the magnitude of this effect will depend upon the rate of rolling-up of the vortex sheets and it would be expected to be most serious at the lower lift coefficients (or higher aspect ratios) where the motions being considered are not of practical concern.

CONCLUDING REMARKS

A detailed analysis has been made of the motions of the four fully rolled-up vortices trailing behind a cruciform wing which is banked 45°. Equations have been developed describing the paths of the four vortices in three dimensions, and calculations have been made of the distance behind the wing at which the upper two vortices leapfrog through the lower two. The latter calculations were confined to wings of triangular plan form. The simplified analysis presented in the early portions of the report has been modified to account for the fact that all the

vorticity shed from the cruciform wing is not actually contained in the four rolled-up vortices.

It was found that the leapfrog distance decreased with increasing lift coefficient and increased with increasing aspect ratio. For angles of attack up to a certain critical value of $C_L/\pi A^2$, the vortex motion is periodic with downstream distance, while above the critical value the motion is aperiodic.

From the fact that the leapfrog phenomenon can occur within two chord lengths of the wing trailing edges, it is clear that downwash calculations even at distances less than one chord length behind low-aspect-ratio cruciform wings must take into account the vortex motions considered in this report. Once the positions of the vortices are known, there are methods available for approximating the downwash, and corrections can be made for the viscous vortex cores by assuming that they rotate as solid bodies.

For angles of bank other than 45°, it is doubtful, due to the lack of symmetry, that calculations of the type presented here could be made by other than numerical procedures.

Ames Aeronautical Laboratory,
National Advisory Committee for Aeronautics,
Moffett Field, Calif., Oct. 5, 1951.

REFERENCES

1. Kaden, H.: Aufwicklung einer unstabilen Unstetigkeitsfläche. Ing. Arch., vol. 2, 1931, pp. 140-168.

2. Spreiter, John R., and Sacks, Alvin H.: The Rolling Up of the Trailing Vortex Sheet and Its Effect on the Downwash Behind Wings. Jour. Aero. Sci., vol. 18, no. 1, Jan. 1951, pp. 21-32.

3. Lanchester, F. W.: Aerodynamics: Constituting the First Volume of a Complete Work on Aerial Flight. Messrs. Constable and Co., London, 1907.

4. Jones, Robert T.: Properties of Low-Aspect-Ratio Pointed Wings at Speeds Below and Above the Speed of Sound. NACA Rep. 835, 1946. (Formerly NACA TN 1032)

5. Heaslet, Max. A., Lomax, Harvard, and Spreiter, John R.: Linearized Compressible-Flow Theory for Sonic Flight Speeds. NACA Rep. 956, 1950. (Formerly NACA TN 1824)

6. Love, A. E. H.: On the Motion of Paired Vortices with a Common Axis. London Math. Soc., Proc., March 8, 1894, pp. 185-194.

7. Hicks, W. M.: On the Mutual Threading of Vortex Rings. Royal Soc. of London, Proc., Series A, 1922, pp. 111-131.

8. Milne-Thomson, L. M.: Theoretical Hydrodynamics. MacMillan and Co., Limited, London, 2d ed., 1950, p. 320.

9. Spreiter, John R.: The Aerodynamic Forces on Slender Plane- and Cruciform-Wing and Body Combinations. NACA Rep. 962, 1950. (Formerly NACA TN 1897)

10. Betz, A.: Behavior of Vortex Systems. NACA TM 713, 1933.

11. Helmholtz, H.: On Integrals of the Hydrodynamical Equations Which Express Vortex Motion. Phil. Mag., vol. XXXIII, 4th series, 1867, pp. 485-511. (Tait's translation from Crelle's Journal, vol. LV, 1858)

12. Jones, Arthur L. and Alksne, Alberta: The Load Distribution Due to Sideslip on Triangular, Trapesoidal, and Related Plan Forms in Supersonic Flow. NACA TN 2007, 1950.

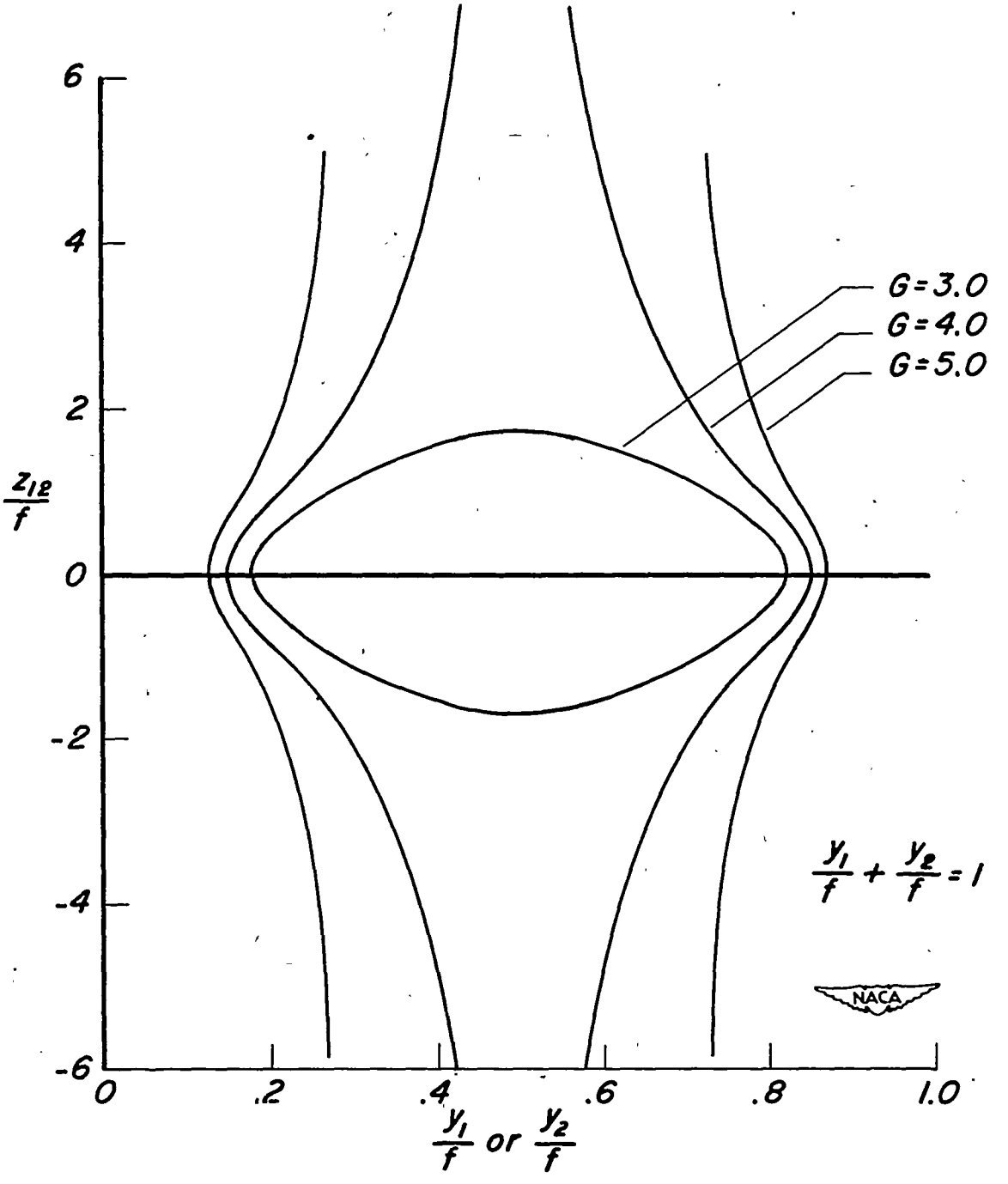

Figure 1.- Relative vortex paths in the yz plane.

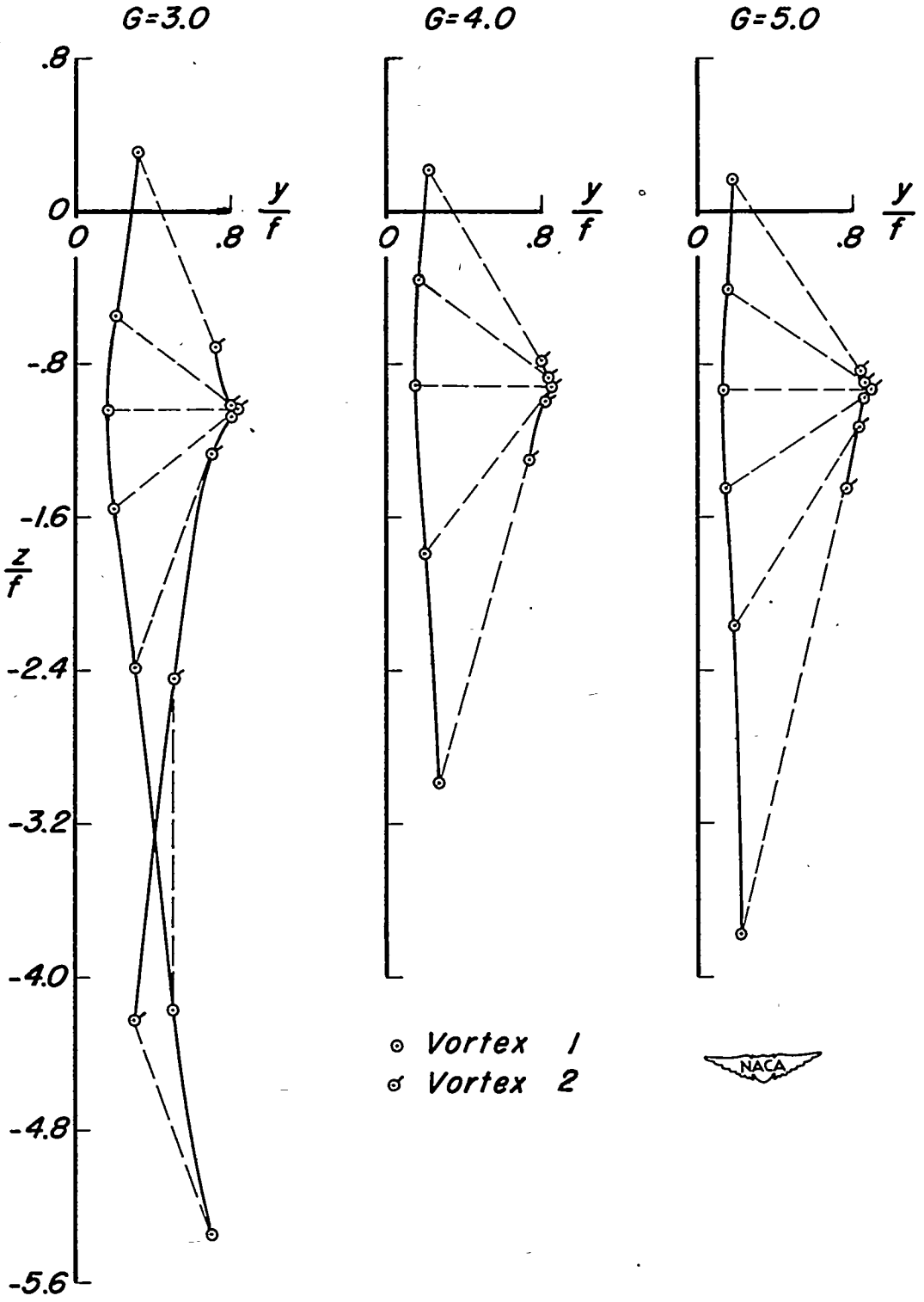

Figure 2.- Vortex paths in the yz plane.

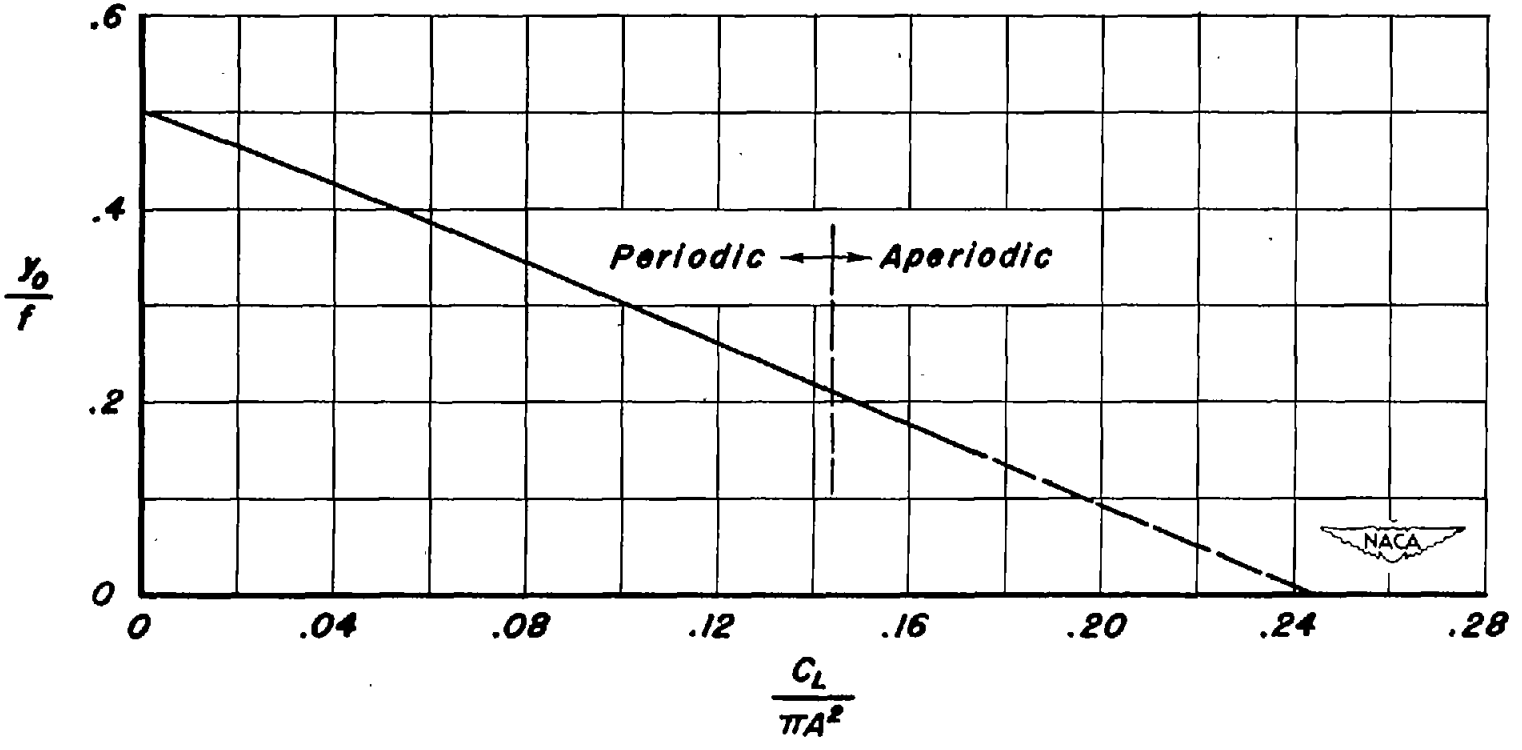

Figure 3.- Variation of initial position of vortex I with lift coefficient.

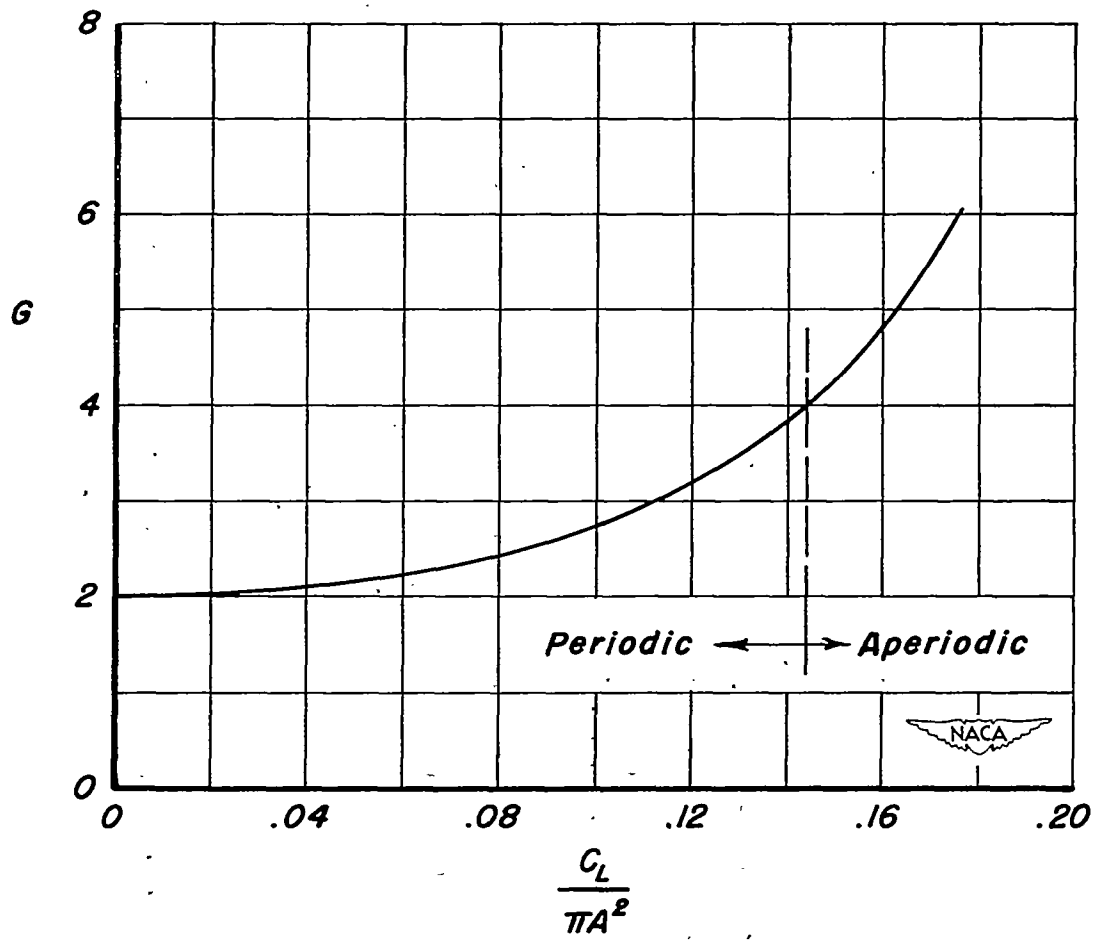

Figure 4.- Variation of parameter G with lift coefficient

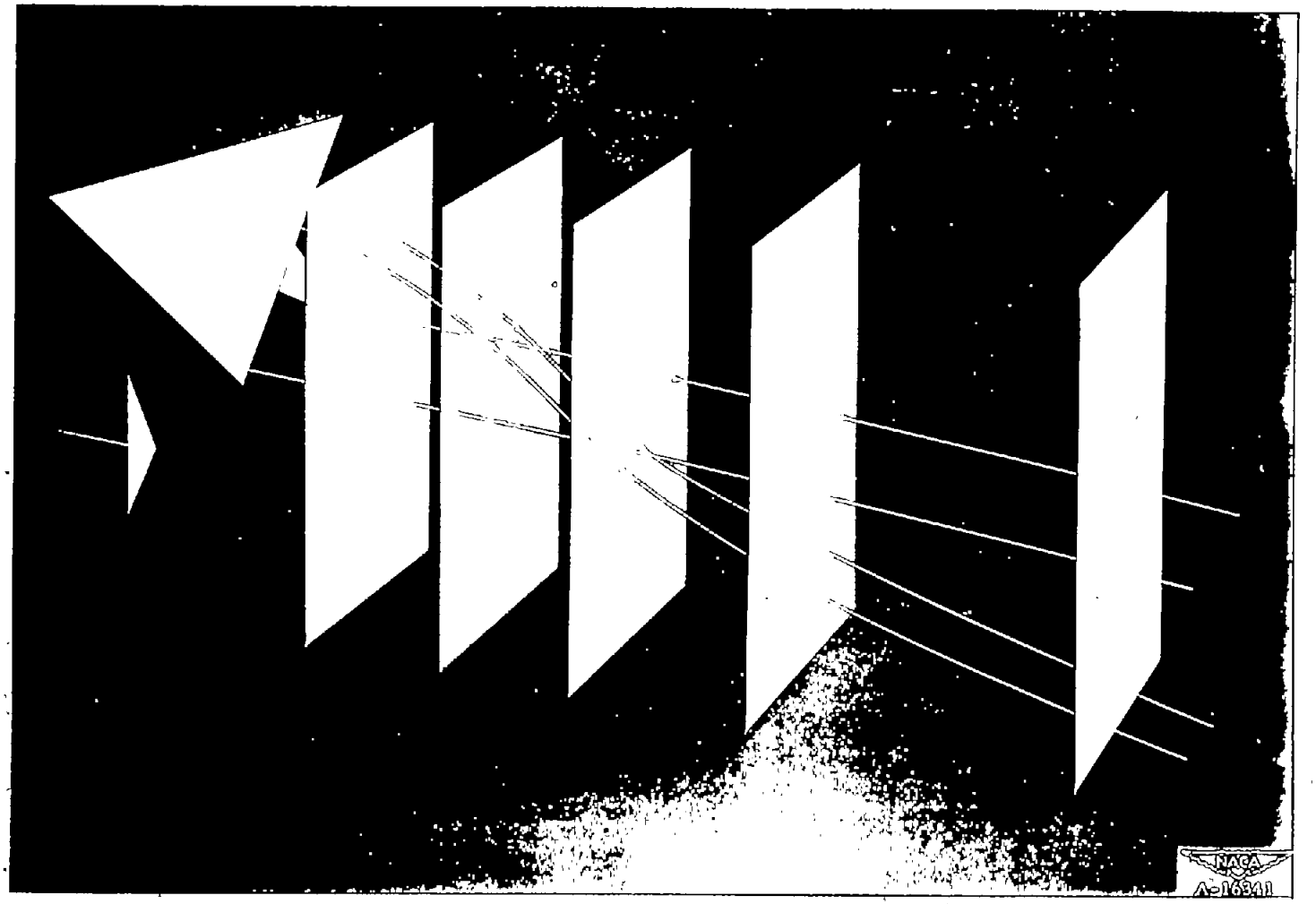

Figure 5.- Typical three-dimensional paths of four vortices trailing behind cruciform wing banked 45°; aspect ratio 2. $C_L = 1.41$.

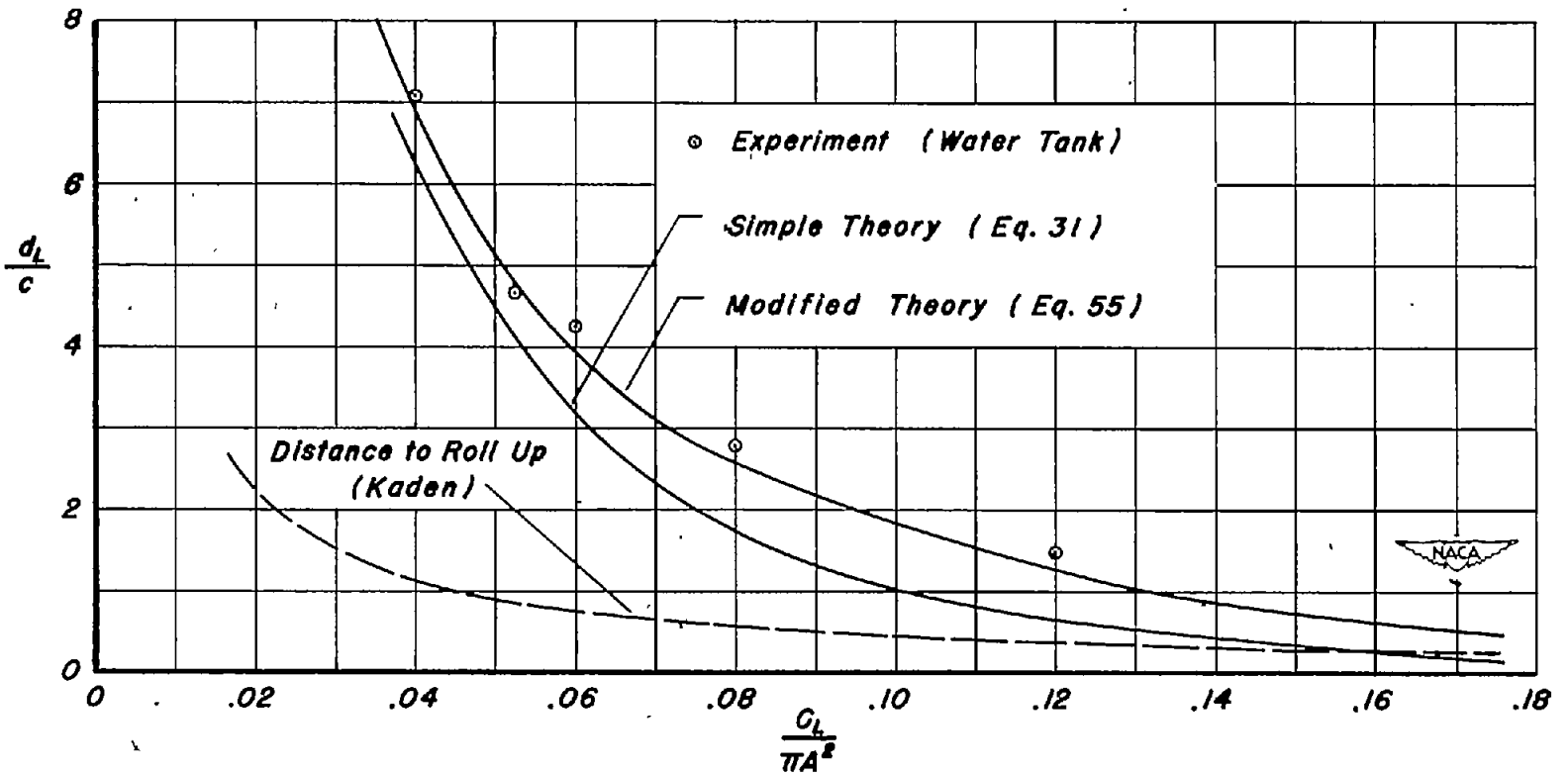

Figure 6.- Variation of leapfrog distance with lift coefficient.

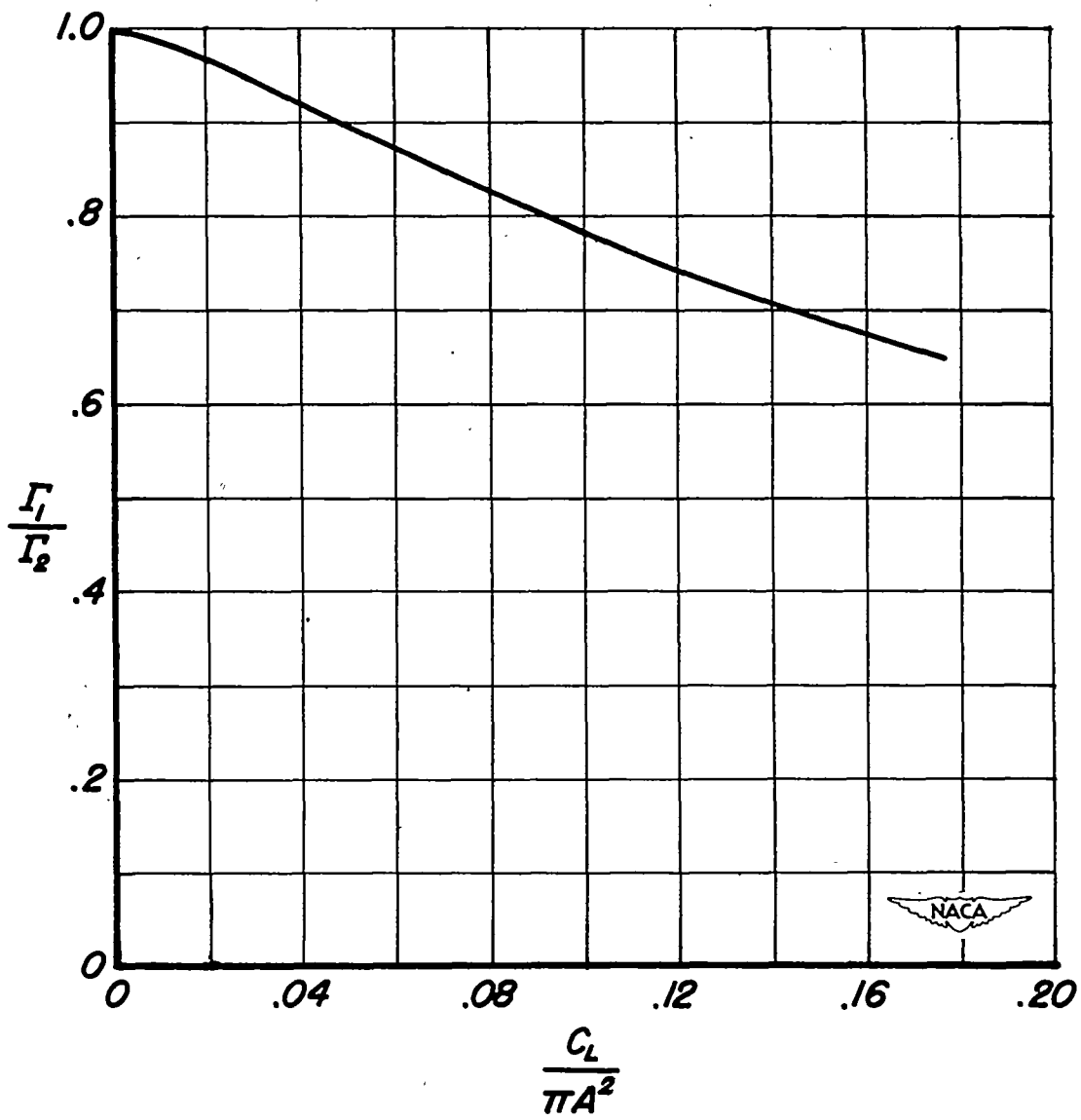

Figure 7.- Variation of relative vortex strengths with lift coefficient.

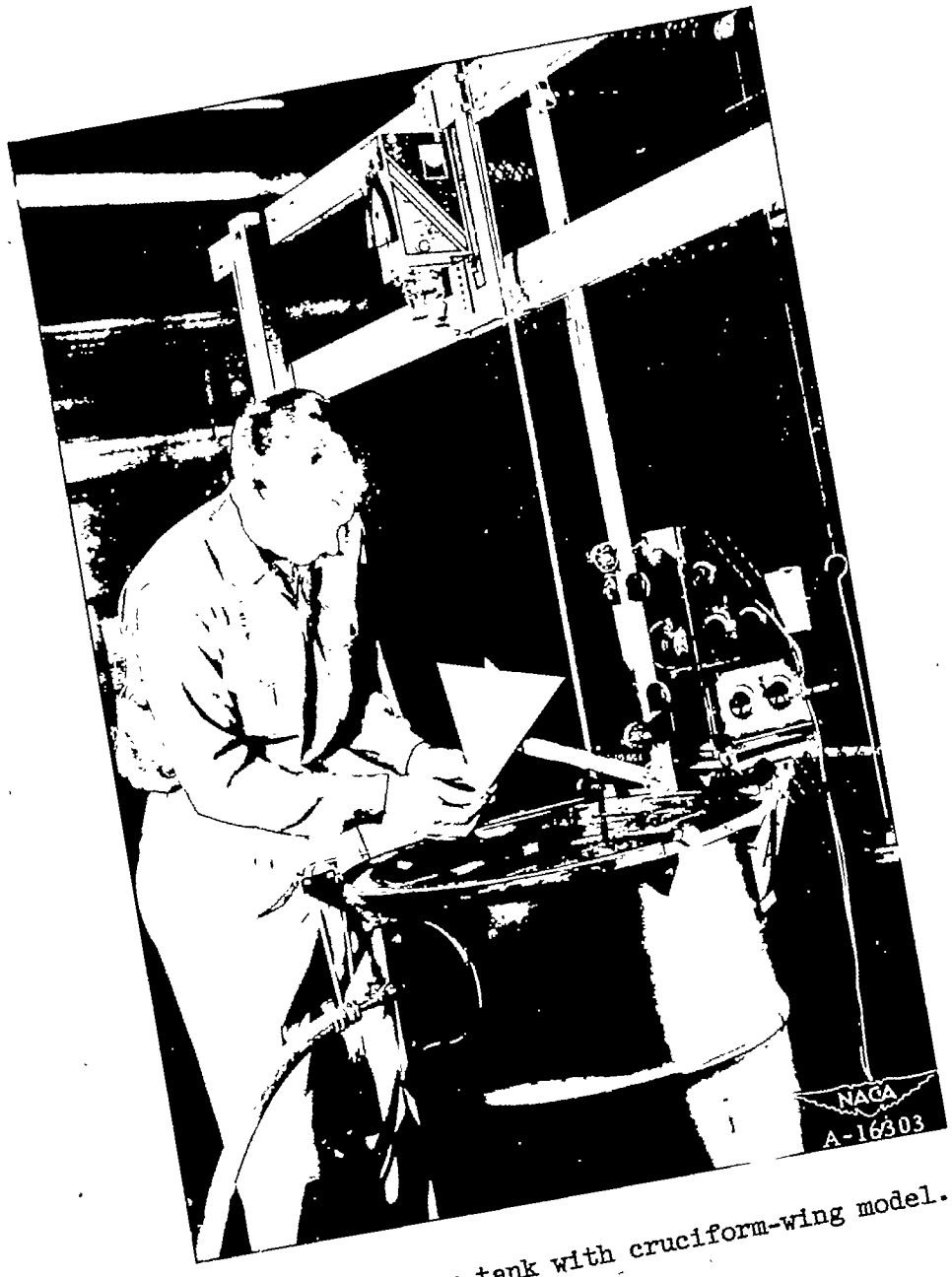

Figure 8.- Water tank with cruciform-wing model.

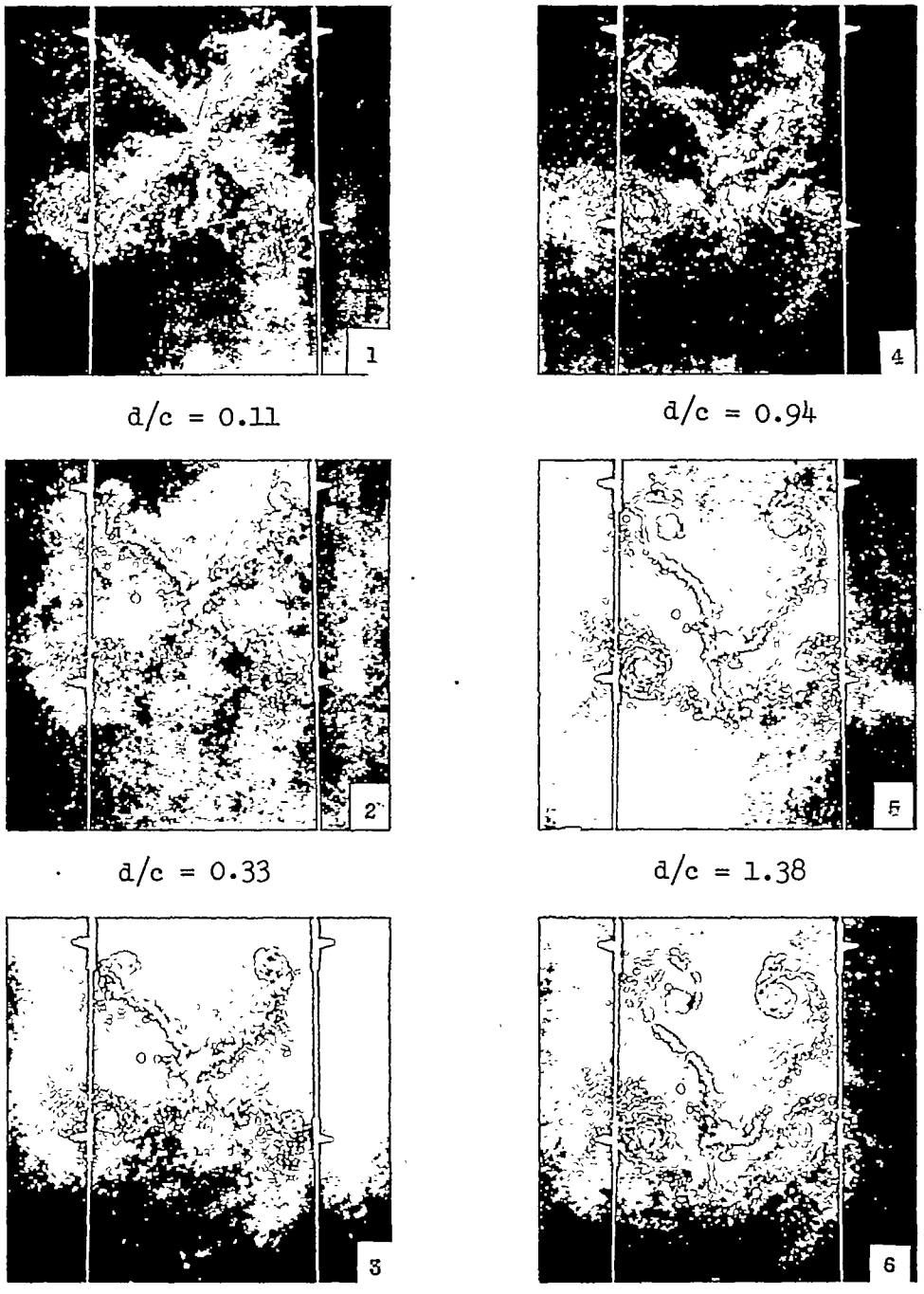

(a) Stations 1 to 6.

Figure 9.- Photographs of wake at various stations behind a triangular cruciform wing of aspect ratio 2. $C_L \approx 0.66$.

d/c = 2.24

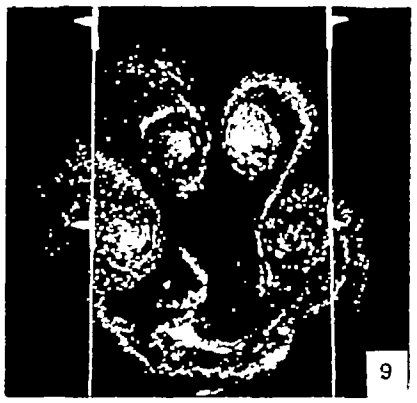

d/c = 3.65

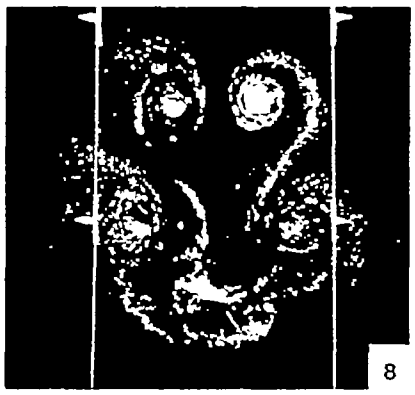

d/c = 2.83

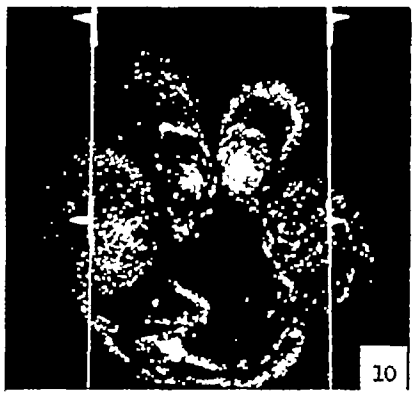

d/c = 4.26

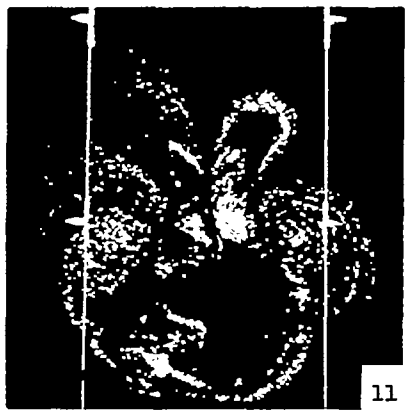

d/c = 4.81

A-16568

(b) Stations 7 to 11.

Figure 9.- Concluded.

NACA-Langley - 1-14-52 - 1000